UCSF

UC San Francisco Previously Published Works

Title

Theranostic Targeting of CUB Domain–Containing Protein 1 (CDCP1) in Multiple Subtypes of Bladder Cancer.

Permalink

https://escholarship.org/uc/item/7c52c4xj

Journal

Clinical Cancer Research, 29(7)

ISSN

1078-0432

Authors

Chopra, Shalini
Trepka, Kai
Sakhamuri, Sasank
et al.

Publication Date

2023-04-03

DOI

10.1158/1078-0432.ccr-22-1973

Peer reviewed

Theranostic targeting of CUB domain containing protein 1 (CDCP1) in multiple subtypes of bladder cancer

Shalini Chopra[1], **Kai Trepka**[2,3], **Sasank Sakhamuri**[1], **Alberto Carretero-González**[3], **Jun Zhu**[3], **Emily Egusa**[3], **Jie Zhou**[4], **Kevin Leung**[4], **Ning Zhao**[1], **Nima Hooshdaran**[1], **Felix Y. Feng**[3,5,6], **James A. Wells**[4,6], **Jonathan Chou**[3,5,6], **Michael J. Evans**[1,4,6]

[1]Department of Radiology and Biomedical Imaging, University of California, San Francisco, San Francisco, CA 94158.

[2]Department of Microbiology and Immunology, University of California, San Francisco, San Francisco, CA 94158.

[3]Department of Radiation Oncology, University of California, San Francisco, San Francisco, CA 94158.

[4]Department of Pharmaceutical Chemistry, University of California, San Francisco, San Francisco, CA 94158.

[5]Department of Medicine, University of California, San Francisco, San Francisco, CA 94158.

[6]Helen Diller Family Comprehensive Cancer Center, University of California, San Francisco, San Francisco, CA 94158.

Abstract

Purpose: Despite recent approvals for checkpoint inhibitors and antibody drug conjugates targeting NECTIN4 or TROP2, metastatic bladder cancer (BC) remains incurable and new treatment strategies are urgently needed. CUB domain containing protein 1 (CDCP1) is a cell surface protein and promising drug target for many cancers. This study aimed to determine whether CDCP1 is expressed in BC and whether CDCP1 can be targeted for treatment with radiolabeled antibodies.

Experimental Design: *CDCP1* expression was evaluated in four BC datasets (n = 1,047 biopsies). A tissue microarray of primary BC biopsies was probed for CDCP1 by immunohistochemistry. CDCP1 expression was evaluated in patient derived xenografts and cell lysates by immunoblot, flow cytometry, and saturation binding assays. Tumor detection in mouse BC models was tested using [89]Zr-labeled 4A06, a monoclonal antibody targeting the ectodomain of CDCP1. [177]Lu-4A06 was applied to mice bearing UMUC3 or HT1376 xenografts to evaluate antitumor effects (CDCP1 expression in UMUC3 is 10 fold higher than HT1376).

Corresponding authors: Michael J. Evans PhD, Address: 600 16th Street, N572C, San Francisco, CA 94158, Telephone: 415-514-1292, michael.evans@ucsf.edu, Jonathan Chou, MD, PhD, Address: 1450 3rd St, Box 3110, San Francisco, CA 94158, jonathan.chou@ucsf.edu.

Statement of Translational Relevance: Metastatic bladder cancer remains incurable and there is an urgent need to develop new therapeutics. Herein, we present the first evidence suggesting that the cell surface tumor antigen CUB domain containing protein 1 (CDCP1) is a viable target for bladder cancer therapy using radiolabeled anti-CDCP1 antibodies. Notably, CDCP1 is overexpressed in tumors that lack TROP2 and/or Nectin-4, which suggests CDCP1 directed therapeutics may add to the current standard of care.

Results: *CDCP1* was highest in the basal/squamous subtype, and CDCP1 was expressed in 53% of primary biopsies. *CDCP1* was not correlated with pathologic or tumor stage, metastatic site, or NECTIN4 and TROP2 at the mRNA or protein level. CDCP1 ranged from $10^5 - 10^6$ receptors per cell. Mechanism studies showed that RAS signaling induced CDCP1 expression. [89]Zr-4A06 PET detected five human bladder cancer xenografts. [177]Lu-4A06 inhibited the growth of UMUC3 and HT1376 xenografts, models with high and moderate CDCP1 expression, respectively.

Conclusions: These data establish that CDCP1 is expressed in BC, including TROP2 and NECTIN4-null disease, and suggest that BC can be treated with CDCP1-targeted radiotherapy.

Keywords

Introduction:

Bladder cancer (BC) is the second most common malignancy of the genitourinary tract, leading to over 17,000 deaths in the US each year (1,2). Despite advances in imaging, chemotherapy, and surgery, the survival of patients who develop metastatic bladder cancer (mBC) remains poor. Treatments for mBC were historically limited to platinum-based chemotherapy, until the approval of the first checkpoint inhibitor in 2016 (3). However, anti-PD1 therapy is only effective in about 25% of patients (4). More recently, two antibody drug conjugates (ADCs), enfortumab vedotin (which targets the surface protein NECTIN4) and sacituzumab govitecan (which targets the surface protein TROP2) received full and accelerated FDA approval, respectively, based on trials conducted in heavily pre-treated patients (5–7). With the milestone FDA approvals, these therapies are now being tested in earlier disease settings.

Muscle-invasive bladder cancer (MIBC) is a molecularly diverse disease and has been classified into six molecular subtypes (8), and it is therefore reasonable to anticipate that not all subtypes may express sufficient TROP2 or NECTIN4 to be vulnerable to the cognate ADCs (estimated to be ~20,000 receptors per cell) (9,10). Consistent with this hypothesis, we recently profiled the six subtypes (11) and showed that NECTIN4 is highly enriched in the luminal subtypes of MIBC, which is critical for drug response, with comparatively lower expression in the 4 other subtypes (9). These data begin to suggest a molecular diversity to MIBC that will likely necessitate a large repertoire of therapeutics targeting other antigens expressed in NECTIN4 or TROP2 null tumors.

Since its cloning in 2001 (12), the cell surface protein CUB domain containing protein 1 (CDCP1) has emerged as a promising target for cancer therapy. The single pass transmembrane protein has been shown to be overexpressed in numerous solid tumor and hematologic malignancies at levels well above the threshold for therapeutic modalities like ADCs and CAR T cell therapy (i.e. ~10^6 receptors/cell) (13,14). Moreover, expression in normal human tissues is generally low, with primarily cytosolic protein expression reported in colon endothelial cells and cell surface expression on CD34+ stem/progenitor cells in bone marrow (15). This restricted tissue expression has led several groups, including our own, to develop antibody-based therapeutics targeting the ectodomain of CDCP1 (16,17).

ADCs, antibody coated liposomes, and radiolabeled antibodies have displayed encouraging antitumor activity in mouse models of pancreatic, ovarian, prostate, colorectal, and breast cancer with limited evidence of host toxicity (13,14,18–21).

Despite the growing interest in CDCP1, virtually nothing is known about its expression in mBC excepting two anecdotes. First, Cantley et al. reported *CDCP1* upregulation in BC primary tumor biopsies compared to matched normal bladder tissue, though the source of the tumor tissues and their corresponding subtypes were not described (22). Second, Ji et al. proposed a model for BC initiation in which N6 methyladenosine modification on *CDCP1* mRNA by methyltransferase like 3 (METTL3) causes CDCP1 overexpression. This knowledge gap, as well as the potential upside of discovering a new cell surface target to treat BC led us to investigate in this study if (1) CDCP1 is overexpressed in BC and in which subtypes, (2) CDCP1 overexpression occurs in TROP2 and/or NECTIN4 null BC tumors, and (3) CDCP1 can be exploited for targeted radiotherapy (TRT) to treat BC.

Material and Methods:

General Methods:

All materials and chemicals were purchased from commercial vendors and used without further processing/purification. HT-1376, HT-1197, 5637, TCCSUP and 639V cells were obtained from the UCSF Cell Culture Facility. UMUC-3, T-24, 253-J, UMUC-9 cells were gifts from Bradley Stohr (UCSF) and David McConkey (Pathology Core, Bladder Cancer SPORE, MD Anderson Cancer Center). Cellular identity was confirmed with short tandem repeat (STR) analysis. Bladder cancer lines were grown in standard MEM media (Life Technologies) supplemented with 10% FBS (Seradigm). Cellular identity was authenticated by visually inspecting morphology and probing for signature expression markers on immunoblot. Mycoplasma was tested after thawing cryostocks with the MycoAlert kit (Lonza). Bladder cancer patient derived xenografts (PDX) were generated at UCSF in collaboration with the Preclinical Therapeutics Core. Sotorasib and trametinib were purchased from MedChemExpress and used without further purification. The monoclonal antibody 4A06 was expressed and purified in the IgG1 format as previously described (18). p-SCN-Bn-Deferoxamine (B-705) and p-SCN-Bn-DOTA (B-205) were purchased from Macrocyclics (Plano, TX) and directly used for conjugation to antibody. ^{89}Zr-oxalate was obtained from 3D Imaging, LLC (Maumelle, AR). ^{177}LuCl$_3$ was obtained from Oak Ridge National Laboratory. Iodine-125 was obtained from Perkin Elmer.

Patient populations and transcriptome profiling:

Four retrospective publicly available cohorts of patients with muscle-invasive bladder cancer were analyzed as previously described (9,10). Briefly, the Sjödahl 2012 (n=93) dataset (obtained from NCBI Gene Expression Omnibus [GEO], accession number GSE32894) had undergone batch effect correction, quantile normalization, log2-transformation, and gene centering by the authors (23). The Sjödahl 2017 (n=243) dataset (obtained from GEO, accession number GSE83586) had been pre-processed including RMA-normalization and gene centering by the authors (24). The TCGA (n=406) dataset (25) was obtained from cBioPortal and had been normalized by RSEM and was further transformed

by log2(RSEM+1), and was renormalized to TPM when undergoing comparisons to healthy patient data (26,27). The Seiler 2017 (n=305) dataset (obtained from GEO, accession number GSE87304) had been SCAN-normalized by the authors (28). The IMvigor210 (n=316 patients, 348 samples) dataset [9] was obtained from http://research-pub.gene.com/IMvigor210CoreBiologies/ and was TPM-normalized and further transformed by log2(TPM+1). For Supplemental Figure 4, cancer spread to the lymph nodes only was classified as locally advanced, while liver or visceral spread was classified as metastatic. These data consisted of de-identified and anonymized gene expression profiles and were deposited into the public domain. All cohorts underwent consensus molecular cluster subtyping as previously described (11). A healthy cohort from the GTEx Consortium was used to investigate normal tissue expression of CDCP1 (29). All further analyses were made in the R statistical environment v4.1.1.

Histology and Immunohistochemistry:

A bladder cancer tissue microarray (TMA), which contains 80 formalin-fixed, paraffin-embedded (FFPE) biopsy specimens in duplicate, was obtained from the University of British Columbia (30). All studies involving human subjects were performed with approval from an Institutional Review Board, and all human studies were conducted in compliance with the Declaration of Helsinki. Written informed consent was obtained prior to collecting the biopsy samples. Sections of FFPE tissue were placed into the Ventana Discovery Ultra automated slide stainer. Antigen retrieval was performed using heat-inactivated antigen retrieval buffer (Tris-EDTA) according to the manufacturer instructions (Roche) and then stained with a rabbit polyclonal CDCP1 primary antibody (Cell Signaling Technology, #4115S, 1:50). Secondary antibodies (Anti-Rabbit HQ and HQ-HRP, from Ventana) were incubated for 12 min each, and DAB was used for detection for single stains. Slides were counterstained with hematoxylin per standard protocol. H-scores for CDCP1 staining were assigned by two independent pathologists (1+, 2+ and 3+ multiplied by the percentage), and the average of the H-scores was calculated.

Flow Cytometry:

Cells were trypsinized and washed, and then incubated with either a PE-anti-CDCP1 antibody (Biolegend #324017, 1:100) or 4A06 for 30 minutes on ice. For cells incubated with unlabeled 4A06, after the 30 min incubation, the cells were washed with PBS multiple times and placed in a fluorophore conjugated secondary antibody solution for 30 minutes on ice (1:1000, 109–546–097, Jackson ImmunoResearch). Cells were collected and washed before being placed in PBS and passed through a cell strainer. Cells were analyzed using an Attune NxT Flow and data were analyzed using FlowJo software.

Immunoblot:

Cell lines and PDX samples were lysed in Pierce RIPA lysis buffer (89900, ThermoFisher Scientific) with protease and phosphatase inhibitors (1861281, ThermoFisher Scientific). The samples were homogenized using a probe sonicator (Omni TH-01) and then centrifuged for 15 minutes at 15,000 x g. After calculating protein concentration using a Bradford Assay kit, 15 µg of lysate was resolved via electrophoresis using a 4–12% Bis Tris gel (NW04120BOX, Invitrogen). Gels were transferred onto an Immobilon-P membrane

(IPVH00010, Millipore). Membranes were blocked in 5% milk in TBST for 30 minutes at room temperature before being placed in a primary antibody solution. The primary antibodies used were anti-CDCP1 (4115, Cell Signaling, 1:1000), TROP2 (214488, abcam, 1:1000), NECTIN4 (17402S, Cell Signaling, 1:1000), and anti-beta actin (A5441, Sigma-Aldrich, 1:5000) or GAPHDH (Cell Signaling #5174). The antibodies were incubated for 1 hour at room temperature or overnight at 4° C. Membranes were then washed with TBST and incubated with a secondary antibody solution for 30 min at room temperature. Secondary antibodies used were goat anti-rabbit (65–6120, Invitrogen, 1:5000), goat anti-rat (62–6520, Invitrogen, 1:5000), or HRP-anti-rabbit (Cell Signaling Technology, #7074). Proteins were detected using West Pico Chemiluminescent Substrate for 20 seconds (34578, ThermoFisher Scientific) and then exposed to film (30–507, Blue Devil). Each immunoblot was reproduced at least once with freshly harvested protein samples.

Saturation binding assays:

^{125}I-4A06 was prepared using our previously reported protocol (14). The final yield of purified ^{125}I-4A06 was ~ 60% (specific activity ~ 1 μCi/μg) and purity was > 99%. UMUC3, TCC SUP, 5637, and UMUC9 cells (0.6×10^6 cell/well) were seeded on 12-well plates using DMEM (10% FBS). The cells were washed with PBS for the saturation binding assay. Total binding of ^{125}I-4A06 was determined by adding it to cell suspensions at seven concentrations from 0.025 nM to 10 nM. Non-specific binding was determined by adding 1000x cold 4A06 to ^{125}I-4A06/cell mixtures at three concentrations. Cells were incubated with ~ 0.5 μCi ^{125}I-4A06 at room temperature for 1 hr, washed with PBS, and lysed by adding 1.0 M NaOH. The bound and unbound radioactive fractions were collected and measured on a Hidex Gamma counter (Turku, FI). Bmax was calculated using Prism v8.0.

Animal studies:

All animal studies were conducted in compliance with Institutional Animal Care and Use Committee at UCSF. For tumor imaging or treatment studies with BC xenografts from cell line implants, six to eight-week-old intact male athymic nu/nu mice (Charles River) were utilized. Mice were inoculated subcutaneously (~1.5×10^6 cells) in the flank with a slurry of cells in 1:1 mixture (v/v) of media and Matrigel (Corning). Xenografts were generally palpable within 3–4 weeks after injection. 4A06 was functionalized with desferrioxamine (DFO) and subsequently radiolabeled with Zr-89 as previously described (14). Tumor-bearing mice received ~300 μCi of ^{89}Zr-4A06 in 100 μL saline solution volume intravenously using a custom mouse tail vein catheter with a 28-gauge needle and a 100–150 mm long polyethylene microtubing. 4A06 was functionalized with DOTA and radiolabeled with Lu-177 as previously described (14). Mice bearing subcutaneous UMUC3 tumors received ^{177}Lu-4A06 (400 μCi) or vehicle (saline) via tail vein at day 0 and day 7 of the study period. Mice bearing subcutaneous HT1376 tumors received ^{177}Lu-4A06 (400 μCi) or vehicle (saline) via tail vein at day 0 and day 7 of the study period. Mice were arranged in treatment arms using a simple randomization approach (31). Animals were weighed at the time of injection, and three times per week until the completion of the study. Tumor volume measurements were calculated at the same time points with calipers. The study endpoints were death due to tumor volume >2000 mm^3 or   20% loss in mouse body weight. The

researcher performing the tumor volume and body weight measurements was blinded to the treatment arms.

Small animal PET/CT:

Mice were imaged on a small animal PET/CT scanner (Inveon, Siemens Healthcare, Malvern, PA). Animals were typically scanned for 30 minutes for PET, and the CT acquisition was performed for 10 minutes. The co-registration between PET and CT images was obtained using the rigid transformation matrix generated prior to the imaging data acquisition since the geometry between PET and CT remained constant for each of PET/CT scans using the combined PET/CT scanner. For microPET/CT data, PET images were reconstructed using the ordered subsets expectation maximization algorithm (OSEM) provided by the scanner manufacturer. The parameters for OSEM were 16 subsets and 4 iterations, and the resulting reconstructed image volume was in a matrix of $128 \times 128 \times 159$ with a voxel size of 0.0776 mm $\times$ 0.0775 mm $\times$ 0.0796 mm. CT images for attenuation correction were reconstructed using a conebeam Feldkamp algorithm provided by the scanner manufacturer. The data were acquired using x-ray tube voltage of 80 kVp and current of 0.5 mA for 120 angular steps over 220 degrees, and 175 ms of exposure at each angular step. The reconstructed CT volume was in a matrix of $512 \times 512 \times 700$ with a voxel size of 0.195 mm $\times$ 0.195 mm $\times$ 0.195 mm. The precalibrated scaling was used to convert the CT images to attenuation maps for correction in PET reconstruction.

For SUV computation, we used freeware software, Amide (amide.sourceforge.net), and used its automated SUV calculation tool by entering decay-corrected injected activity and the animal weight. For each volume of interest, a spherical VOI (2–3 mm diameter) was drawn and SUV was calculated by VOI statistics.

Biodistribution studies:

At a dedicated time after radiotracer injection, animals were euthanized by cervical dislocation. Blood was harvested via cardiac puncture. Tissues were removed, weighed, and counted on a Hidex automatic gamma counter (Turku, Finland). The activity of the injected radiotracer was calculated and used to determine the total number of counts per minute by comparison with a standard of known activity. The data were background- and decay-corrected and expressed as the percentage of the injected dose/weight of the biospecimen in grams (%ID/g).

Statistical analysis:

For the transcriptomic analysis, correlation was calculated by Spearman's rank correlation. ANOVA and Kruskal-Wallis tests were used to test for differences when there were more than two groups, and the Wilcoxon rank-sum test was used to test for differences between two groups unless otherwise stated. Binary comparisons between two treatment arms were made with an unpaired, two-tailed Student's t-test. Differences at the 95% confidence level ($P < 0.05$) were considered statistically significant. Unless otherwise stated, all data were expressed as mean ± standard deviation. Kaplan–Meier survival analyses using log-rank testing were performed on quartiles of *CDCP1* mRNA expression with overall survival as the endpoint.

Data availability:

All data are available upon request from the corresponding authors of this study.

Results

CDCP1 is expressed in all molecular subtypes of BC, with the highest expression in the basal/squamous subtype.

To assess *CDCP1* mRNA expression across the molecular subtypes of MIBC, we analyzed four cohorts of patients with localized, muscle-invasive bladder tumors (23–25,28). The clinical characteristics of these cohorts were previously described (32). Using the consensus classifier subtypes (11), we found that median CDCP1 expression was elevated in the basal/squamous (Ba/Sq) subtype of muscle-invasive bladder cancer relative to the luminal (LumP, LumNS and LumU), stromal-rich and neuroendocrine (NE)-like subtypes (Figure 1A–D and Supplemental Table 1). To determine whether CDCP1 is enriched in patients with bladder cancer, we also compared median expression of CDCP1 in healthy patients to expression of CDCP1 in a similarly normalized dataset of patients with MIBC (25). We validated our findings that CDCP1 protein was enriched in Ba/Sq tumors by immunohistochemistry (IHC) using a previously described tissue microarray (TMA) (30) (Figure 1E–F). We found that *CDCP1* mRNA expression and CDCP1 protein expression were broadly observed across clinical stages and pathological subtypes. There was not enrichment of CDCP1 expression in any single subtype or clinical stage (Supplemental Figures 1–3). In addition, *CDCP1* mRNA was mutually expressed in patients with locally-advanced versus metastatic disease, and did not vary significantly between the primary bladder or metastatic biopsy site (Supplemental Figures 4–5). Lastly, no significant associations between quartiles of CDCP1 expression and overall survival were seen in cohorts for which retrospective clinical data were available (Supplemental Figure 6).

We next evaluated CDCP1 protein expression in human bladder cancer cell lines representing luminal (5637, HT-1197, HT-1376, UMUC9) and basal subtypes (639V, T24, 253JBV, UMUC3, TCCSUP). Cell surface protein expression was observed in all cell lines by flow cytometry using 4A06, a monoclonal antibody we previously developed to target the ectodomain of CDCP1 (18) (Figure 2A). UMUC3 and TCC SUP had the highest expression of CDCP1, while UMUC9 and 253 JBV had the lowest relative level. We further quantified cell surface receptor numbers using ^{125}I-labeled 4A06. Saturation binding assays showed that UMUC3 and TCCSUP had ~1×10^6 receptors per cell, while UMUC9, HT1376 and 5637 had ~1×10^5 receptors per cell (Table 1 and Supplemental Figure 7).

CDCP1 is expressed in TROP2 and NECTIN4-low and null BC.

Full length CDCP1 (~140 kDa) can be proteolytically cleaved on the cell surface to generate a truncated form (~90 kDa), and some recent studies have suggested either form promotes cancer aggressiveness through discrete mechanisms (19,33). On this basis, we next evaluated CDCP1 expression on immunoblot. Full length and cleaved CDCP1 were detected in cell lines (Figure 2B). In general, full length CDCP1 was equivalently or more abundantly expressed than cleaved CDCP1. In one cell line, 5637, cleaved CDCP1 was more abundant that full length. Interestingly, we found that CDCP1 was robustly expressed in UMUC3,

T24, 639V and TCCSUP lines, which are all negative for NECTIN4 and TROP2; our previous work demonstrated that these NECTIN4[NEG] and TROP2[NEG] cells lines are not effectively targeted by enfortumab vedotin (EV) or sacituzumab govitecan (SG) (9,10). In addition, CDCP1 was detected in three of five bladder PDX samples (Figure 2C). To understand the relationship between CDCP1, NECTIN4 and TROP2 more broadly, we analyzed the expression correlations between these genes. Across all four datasets, we found that *CDCP1* expression was either not correlated or inversely correlated with both *NECTIN4* and *TROP2* expression (Figure 2D and Supplemental Figure 8).

CDCP1 can be targeted on BC tumors for nuclear imaging and therapy with radiolabeled antibodies.

To understand if CDCP1 can be exploited for BC therapy, we next assessed the tumoral uptake of 4A06, a recombinant human monoclonal antibody we previously developed against an extracellular epitope contained on both full length and cleaved CDCP1 (18). 4A06 was functionalized with desferrioxamine and radiolabeled with Zr-89 as previously described (14,18). PET and biodistribution studies were conducted at 72 hours post injection of ^{89}Zr-4A06, as we have previously shown peak tumor to background values at this time point (14). We assessed radiotracer uptake in five human xenograft models representing higher (UMUC3, T24, HT1376) and relatively lower (UMUC9, 5637) CDCP1 expression in vitro. Both on PET and *ex vivo* biodistribution, relative levels of ^{89}Zr-4A06 uptake in tumors aligned with the relative CDCP1 expression in vitro (Figure 3A and 3B). The highest tumoral uptake of ^{89}Zr-4A06 was observed in UMUC3 tumors at ~20% ID/g. In all cases, the tumor to background ratio was > 1 (Figure 3C).

We next tested if CDCP1-directed targeted radiotherapy (TRT) could be applied to treat bladder cancer tumors. We chose to prioritize TRT for several reasons. First, TRT has a straightforward mechanism of action, requiring only antigen overexpression. Second, TRT is agnostic to protein function, which is important as a functional role for CDCP1 overexpression in bladder cancer has yet to be determined (34). Second, TRT is undergoing a clinical and commercial renaissance for cancer therapy, and the recent FDA approvals of Lutathera (^{177}Lu-DOTATATE) for neuroendocrine tumors, Azedra (^{131}I-MIBG) for pediatric malignancies, and Pluvicto (^{177}Lu-PSMA 617) for prostate cancer patients fully underscore that TRT can be effective against biologically diverse metastatic solid tumor types (35–37). Lastly, in contrast to other antibody-based therapeutic modalities, TRT using alpha or beta emitting radioisotopes has the competitive advantage of irradiation tumor cells not directly engaged by drug (the so-called "cross-fire effect"). We hypothesize this feature of TRT will be particularly beneficial for treating heterogeneous tumor types like BC.

To test the antitumor effects of RLT, 4A06 IgG1 was first conjugated to the chelator 1,4,7,10-tetraazacyclododecane-1,4,7,10-tetraacetic acid (DOTA) as described before (14). DOTA-4A06 was radiolabeled with Lu-177 using our previously reported protocol. ^{177}Lu-4A06 was administered intravenously in two doses (400 μCi/dose) on day 0 and day 7 of the study period to mice bearing subcutaneous UMUC3 tumors. Treatment with ^{177}Lu-4A06 significantly suppressed tumor growth compared to vehicle controls (Figure 4A and Supplemental Figure 9). Notably, four of nine tumors in the treated arm underwent

a complete response with no tumor outgrowth even at 120 days post injection. Assessing the entire cohort, [177]Lu-4A06 significantly extended survival compared to the control arm (Figure 4B). Mice receiving vehicle had a median survival of 13 days, while mice receiving [177]Lu-4A06 had a median survival of 24 days (Hazard ratio = 4, P< 0.001). The therapy was also well tolerated and no mice in the treatment arm experienced unsafe weight losses (Figure 4C). Lastly, to evaluate antitumor effects in a BC tumor model with at least 10 fold lower CDCP1 expression, mice with subcutaneous HT-1376 tumors were treated with vehicle or [177]Lu-4A06. Mice received two doses (400 μCi/dose) on day 0 and day 7 of the study period. [177]Lu-4A06 treatment significantly reduced tumor growth compared to vehicle by day 28 (Figure 4D and Supplemental Figure 10).

Hyperactive RAS signaling promotes CDCP1 overexpression in BC cells.

Lastly, we carried out an exploratory study to begin probing the mechanisms driving CDCP1 overexpression in BC. RAS/Raf/MEK signaling has been previously shown to induce expression of CDCP1 in other cancers (Figure 5A) (38). Hyperactive RAS signaling is a relatively common feature of BC due to mutations in RAS isoforms, upstream RAS inducers, and downstream effectors (Figure 5B); therefore, we tested if this pathway regulates CDPC1 in BC. Treatment of UMUC3 cells (which harbor a KRAS G12C mutation) with G12C inhibitor sotorasib for 48 hours suppressed CDCP1 expression in a dose dependent fashion on immunoblot and flow cytometry (Figure 5C–D). Treatment of UMUC3 cells the MEK inhibitor trametinib for 48 hours also suppressed CDCP1 expression in a dose dependent fashion on immunoblot and flow cytometry (Figure 5E–F). These data, while preliminary, underscore a potential role for CDCP1 directed therapeutics in mutant RAS BC.

Discussion

In this report, we provide evidence in support of targeting the cell surface antigen CDCP1 to treat BC. Profiling mRNA and protein expression in BC biopsies showed that CDCP1 is expressed in all of the consensus subtypes, with the highest levels found in the aggressive basal/squamous subtype and lowest levels in the NE-like subtype. Flow cytometry and saturation binding studies confirmed that CDCP1 is expressed on the cell surface of both basal and luminal human bladder cancer cell lines. Saturation binding studies in cell line models showed a range of overexpression from $10^5 – 10^6$ receptors per cell. Immunoblot of human BC cell lines and PDX samples demonstrated that both full length and cleaved CDCP1 are expressed.

Interestingly, we found robust CDCP1 expression in several NECTIN4 and TROP2 negative BC lines, suggesting that CDCP1-directed therapies may benefit a different molecular subset of patients, given that antigen expression is one of the key determinants of therapeutic response to currently approved antibody-drug conjugates (39,40). PET/CT studies with [89]Zr-4A06 detected tumor autonomous expression of CDCP1 in four human bladder cancer models of either basal or luminal histology. An antitumor assessment study showed that [177]Lu-4A06 potently suppressed the growth of UMUC3 tumors compared to vehicle controls and extended overall survival. Of note, we observed durable complete responses

in 44% of the mice (four of nine) in the [177]Lu-4A06 treated cohort. Furthermore, we showed that a similar dosing schema for [177]Lu-4A06 suppressed the growth of HT1376 tumors, a model with 10 fold lower expression of CDPC1 compared to UMUC3. Perhaps unsurprisingly, the antitumor effects were less dramatic than what was observed in the UMUC3 cohort, and no mice were cured. More generally, these data add to an ongoing narrative spanning several antitumor assessment studies in mouse models of prostate and pancreatic cancer showing that $\sim 10^5$ receptors per cell are required for durable responses to [177]Lu-4A06 IgG (14,19,41).

While our data demonstrate that CDCP1 overexpression can be a unifying feature of otherwise molecularly diverse BC subtypes, the mechanisms driving this overexpression remains to be elucidated. Our preliminary mechanism studies reaffirmed a role for RAS hyperactivity in promoting CDCP1 overexpression, which likely accounts for the high expression found in RAS mutant cell lines like UMUC3, T24 (HRAS G12V), and 639V (HRAS G12D). However, we also observed high CDCP1 expression in several cell lines that lack RAS hyperactivity, for example TCC SUP, HT-1197, and HT-1397. In these cases, other drivers of CDCP1 may be relevant. More generally, CDCP1 can be induced by numerous oncogenic signaling events relevant to BC including HER2, EGFR and PDGFR, and tumor microenvironment effects like hypoxia (42). We are currently working through these candidates to better define the mechanisms that promote CDCP1 overexpression in BC.

Our study has several important limitations. Firstly, our gene expression data in >1,000 clinical samples may not necessarily reflect CDCP1 surface protein expression (although we have validated the surface protein expression by IHC using a TMA and in cell line models with flow cytometry). Secondly, due to data availability, the samples analyzed in these cohorts were obtained from primary tumor tissue and may not necessarily represent expression levels in metastatic tumors. Additional study of biopsies harvested from metastatic sites is needed to better characterize the similarities and differences in CDCP1 expression between primary tumors and metastases. Also, there may be intra-patient heterogeneity of expression amongst different metastatic lesions that is underappreciated when profiling single biopsies. Lastly, we have performed one antitumor assessment study using a model with the highest CDCP1 expression among the panel. While the data show significant inhibition and even ablation of a highly proliferative tumor model, the study in its current form does not present additional tumor replicates and does not address the minimum level of CDCP1 expression required for CDCP1-directed TRT to be effective.

Our results showing potent inhibition of an aggressive BC xenograft model support revisiting TRT-directed therapies for localized and advanced BC. Indeed, TRT has been sporadically investigated as a treatment option for BC over the past 30 years. As early as the 1990s, several groups demonstrated that radiolabeled antibodies targeting the cell surface proteins TROP1 (also known as HMFG2) and MUC1 (as known as AUA1 antigen) accumulated in superficial primary bladder tumors at high levels above background (43–45). More recently, an anti-EGFR antibody was coupled to the alpha emitter Bi-213 and safely administered by intravesical infusion to 12 patients with carcinoma in situ (46). Notably, 11 of 12 patients had complete responses or stable disease 8 weeks after instillation. We

are optimistic that our data, combined with these prior clinical experiences, will provide a compelling rationale to advance TRTs into clinical trials for patients with both localized and metastatic disease.

Supplementary Material

Refer to Web version on PubMed Central for supplementary material.

Acknowledgements

Conflicts of Interest:

J.A.W. is a co-inventor of patents describing the antibodies targeting CDCP1. J.A.W. receives research support from Bristol Myer Squibb. J.A.W., M.J.E., and J.C. are co-inventors on a patent filing describing radiolabeled CDCP1 antibodies and their use as cancer detection and treatment agents.

References

1. Siegel RL, Miller KD, Fuchs HE, Jemal A. Cancer Statistics, 2021. CA Cancer J Clin 2021;71(1):7–33 doi 10.3322/caac.21654. [PubMed: 33433946]

2. Lenis AT, Lec PM, Chamie K, Mshs MD. Bladder Cancer: A Review. JAMA 2020;324(19):1980–91 doi 10.1001/jama.2020.17598. [PubMed: 33201207]

3. Rosenberg JE, Hoffman-Censits J, Powles T, van der Heijden MS, Balar AV, Necchi A, et al. Atezolizumab in patients with locally advanced and metastatic urothelial carcinoma who have progressed following treatment with platinum-based chemotherapy: a single-arm, multicentre, phase 2 trial. Lancet 2016;387(10031):1909–20 doi 10.1016/S0140-6736(16)00561-4. [PubMed: 26952546]

4. Tran L, Xiao JF, Agarwal N, Duex JE, Theodorescu D. Advances in bladder cancer biology and therapy. Nat Rev Cancer 2021;21(2):104–21 doi 10.1038/s41568-020-00313-1. [PubMed: 33268841]

5. Rosenberg JE, O'Donnell PH, Balar AV, McGregor BA, Heath EI, Yu EY, et al. Pivotal Trial of Enfortumab Vedotin in Urothelial Carcinoma After Platinum and Anti-Programmed Death 1/Programmed Death Ligand 1 Therapy. J Clin Oncol 2019;37(29):2592–600 doi 10.1200/JCO.19.01140. [PubMed: 31356140]

6. Tagawa ST, Balar AV, Petrylak DP, Kalebasty AR, Loriot Y, Flechon A, et al. TROPHY-U-01: A Phase II Open-Label Study of Sacituzumab Govitecan in Patients With Metastatic Urothelial Carcinoma Progressing After Platinum-Based Chemotherapy and Checkpoint Inhibitors. J Clin Oncol 2021:JCO2003489 doi 10.1200/JCO.20.03489.

7. Powles T, Rosenberg JE, Sonpavde GP, Loriot Y, Duran I, Lee JL, et al. Enfortumab Vedotin in Previously Treated Advanced Urothelial Carcinoma. N Engl J Med 2021;384(12):1125–35 doi 10.1056/NEJMoa2035807. [PubMed: 33577729]

8. Choi W, Porten S, Kim S, Willis D, Plimack ER, Hoffman-Censits J, et al. Identification of distinct basal and luminal subtypes of muscle-invasive bladder cancer with different sensitivities to frontline chemotherapy. Cancer Cell 2014;25(2):152–65 doi 10.1016/j.ccr.2014.01.009. [PubMed: 24525232]

9. Chu CE, Sjostrom M, Egusa EA, Gibb EA, Badura ML, Zhu J, et al. Heterogeneity in NECTIN4 Expression Across Molecular Subtypes of Urothelial Cancer Mediates Sensitivity to Enfortumab Vedotin. Clin Cancer Res 2021;27(18):5123–30 doi 10.1158/1078-0432.CCR-20-4175. [PubMed: 34108177]

10. Chou J, Trepka K, Sjostrom M, Egusa EA, Chu CE, Zhu J, et al. TROP2 Expression Across Molecular Subtypes of Urothelial Carcinoma and Enfortumab Vedotin-resistant Cells. Eur Urol Oncol 2022 doi 10.1016/j.euo.2021.11.005.

11. Kamoun A, de Reynies A, Allory Y, Sjodahl G, Robertson AG, Seiler R, et al. A Consensus Molecular Classification of Muscle-invasive Bladder Cancer. Eur Urol 2020;77(4):420–33 doi 10.1016/j.eururo.2019.09.006. [PubMed: 31563503]

12. Scherl-Mostageer M, Sommergruber W, Abseher R, Hauptmann R, Ambros P, Schweifer N. Identification of a novel gene, CDCP1, overexpressed in human colorectal cancer. Oncogene 2001;20(32):4402–8 doi 10.1038/sj.onc.1204566. [PubMed: 11466621]

13. Zhao N, Chopra S, Trepka K, Wang YH, Sakhamuri S, Hooshdaran N, et al. CUB domain containing protein 1 (CDCP1) is a target for radioligand therapy in castration resistant prostate cancer including PSMA null disease. Clin Cancer Res 2022 doi 10.1158/1078-0432.CCR-21-3858.

14. Moroz A, Wang YH, Sharib JM, Wei J, Zhao N, Huang Y, et al. Theranostic Targeting of CUB Domain Containing Protein 1 (CDCP1) in Pancreatic Cancer. Clin Cancer Res 2020;26(14):3608–15 doi 10.1158/1078-0432.CCR-20-0268. [PubMed: 32341034]

15. Conze T, Lammers R, Kuci S, Scherl-Mostageer M, Schweifer N, Kanz L, et al. CDCP1 is a novel marker for hematopoietic stem cells. Ann N Y Acad Sci 2003;996:222–6 doi 10.1111/j.1749-6632.2003.tb03249.x. [PubMed: 12799299]

16. Khan T, Kryza T, Lyons NJ, He Y, Hooper JD. The CDCP1 Signaling Hub: A Target for Cancer Detection and Therapeutic Intervention. Cancer Res 2021;81(9):2259–69 doi 10.1158/0008-5472.CAN-20-2978. [PubMed: 33509939]

17. Uekita T, Sakai R. Roles of CUB domain-containing protein 1 signaling in cancer invasion and metastasis. Cancer Sci 2011;102(11):1943–8 doi 10.1111/j.1349-7006.2011.02052.x. [PubMed: 21812858]

18. Martinko AJ, Truillet C, Julien O, Diaz JE, Horlbeck MA, Whiteley G, et al. Targeting RAS-driven human cancer cells with antibodies to upregulated and essential cell-surface proteins. Elife 2018;7 doi 10.7554/eLife.31098.

19. Lim SA, Zhou J, Martinko AJ, Wang YH, Filippova EV, Steri V, et al. Targeting a proteolytic neoepitope on CUB domain containing protein 1 (CDCP1) for RAS-driven cancers. J Clin Invest 2022;132(4) doi 10.1172/JCI154604.

20. Kryza T, Khan T, Puttick S, Li C, Sokolowski KA, Tse BW, et al. Effective targeting of intact and proteolysed CDCP1 for imaging and treatment of pancreatic ductal adenocarcinoma. Theranostics 2020;10(9):4116–33 doi 10.7150/thno.43589. [PubMed: 32226543]

21. Alajati A, D'Ambrosio M, Troiani M, Mosole S, Pellegrini L, Chen J, et al. CDCP1 overexpression drives prostate cancer progression and can be targeted in vivo. J Clin Invest 2020;130(5):2435–50 doi 10.1172/JCI131133. [PubMed: 32250342]

22. Emerling BM, Benes CH, Poulogiannis G, Bell EL, Courtney K, Liu H, et al. Identification of CDCP1 as a hypoxia-inducible factor 2alpha (HIF-2alpha) target gene that is associated with survival in clear cell renal cell carcinoma patients. Proc Natl Acad Sci U S A 2013;110(9):3483–8 doi 10.1073/pnas.1222435110. [PubMed: 23378636]

23. Sjodahl G, Lauss M, Lovgren K, Chebil G, Gudjonsson S, Veerla S, et al. A molecular taxonomy for urothelial carcinoma. Clin Cancer Res 2012;18(12):3377–86 doi 10.1158/1078-0432.CCR-12-0077-T. [PubMed: 22553347]

24. Sjodahl G, Eriksson P, Liedberg F, Hoglund M. Molecular classification of urothelial carcinoma: global mRNA classification versus tumour-cell phenotype classification. J Pathol 2017;242(1):113–25 doi 10.1002/path.4886. [PubMed: 28195647]

25. Robertson AG, Kim J, Al-Ahmadie H, Bellmunt J, Guo G, Cherniack AD, et al. Comprehensive Molecular Characterization of Muscle-Invasive Bladder Cancer. Cell 2017;171(3):540–56 e25 doi 10.1016/j.cell.2017.09.007.

26. Gao J, Aksoy BA, Dogrusoz U, Dresdner G, Gross B, Sumer SO, et al. Integrative analysis of complex cancer genomics and clinical profiles using the cBioPortal. Sci Signal 2013;6(269):pl1 doi 10.1126/scisignal.2004088.

27. Cerami E, Gao J, Dogrusoz U, Gross BE, Sumer SO, Aksoy BA, et al. The cBio cancer genomics portal: an open platform for exploring multidimensional cancer genomics data. Cancer Discov 2012;2(5):401–4 doi 10.1158/2159-8290.CD-12-0095. [PubMed: 22588877]

28. Seiler R, Ashab HAD, Erho N, van Rhijn BWG, Winters B, Douglas J, et al. Impact of Molecular Subtypes in Muscle-invasive Bladder Cancer on Predicting Response and Survival after Neoadjuvant Chemotherapy. Eur Urol 2017;72(4):544–54 doi 10.1016/j.eururo.2017.03.030. [PubMed: 28390739]

29. Consortium GT. The GTEx Consortium atlas of genetic regulatory effects across human tissues. Science 2020;369(6509):1318–30 doi 10.1126/science.aaz1776. [PubMed: 32913098]

30. Seiler R, Gibb EA, Wang NQ, Oo HZ, Lam HM, van Kessel KE, et al. Divergent Biological Response to Neoadjuvant Chemotherapy in Muscle-invasive Bladder Cancer. Clin Cancer Res 2019;25(16):5082–93 doi 10.1158/1078-0432.CCR-18-1106. [PubMed: 30224344]

31. Altman DG, Bland JM. Statistics notes. Treatment allocation in controlled trials: why randomise? BMJ 1999;318(7192):1209 doi 10.1136/bmj.318.7192.1209. [PubMed: 10221955]

32. Chu CE, Sjostrom M, Egusa EA, Gibb EA, Badura ML, Zhu J, et al. Heterogeneity in NECTIN4 expression across molecular subtypes of urothelial cancer mediates sensitivity to enfortumab vedotin. Clin Cancer Res 2021 doi 10.1158/1078-0432.CCR-20-4175.

33. He Y, Wortmann A, Burke LJ, Reid JC, Adams MN, Abdul-Jabbar I, et al. Proteolysis-induced N-terminal ectodomain shedding of the integral membrane glycoprotein CUB domain-containing protein 1 (CDCP1) is accompanied by tyrosine phosphorylation of its C-terminal domain and recruitment of Src and PKCdelta. J Biol Chem 2010;285(34):26162–73 doi 10.1074/jbc.M109.096453. [PubMed: 20551327]

34. Sgouros G, Bodei L, McDevitt MR, Nedrow JR. Radiopharmaceutical therapy in cancer: clinical advances and challenges. Nat Rev Drug Discov 2020;19(9):589–608 doi 10.1038/s41573-020-0073-9. [PubMed: 32728208]

35. Strosberg J, El-Haddad G, Wolin E, Hendifar A, Yao J, Chasen B, et al. Phase 3 Trial of (177)Lu-Dotatate for Midgut Neuroendocrine Tumors. N Engl J Med 2017;376(2):125–35 doi 10.1056/NEJMoa1607427. [PubMed: 28076709]

36. Sartor O, de Bono J, Chi KN, Fizazi K, Herrmann K, Rahbar K, et al. Lutetium-177-PSMA-617 for Metastatic Castration-Resistant Prostate Cancer. N Engl J Med 2021;385(12):1091–103 doi 10.1056/NEJMoa2107322. [PubMed: 34161051]

37. Hofman MS, Emmett L, Sandhu S, Iravani A, Joshua AM, Goh JC, et al. [(177)Lu]Lu-PSMA-617 versus cabazitaxel in patients with metastatic castration-resistant prostate cancer (TheraP): a randomised, open-label, phase 2 trial. Lancet 2021;397(10276):797–804 doi 10.1016/S0140-6736(21)00237-3. [PubMed: 33581798]

38. Uekita T, Fujii S, Miyazawa Y, Iwakawa R, Narisawa-Saito M, Nakashima K, et al. Oncogenic Ras/ERK signaling activates CDCP1 to promote tumor invasion and metastasis. Mol Cancer Res 2014;12(10):1449–59 doi 10.1158/1541-7786.MCR-13-0587. [PubMed: 24939643]

39. Coates JT, Sun S, Leshchiner I, Thimmiah N, Martin EE, McLoughlin D, et al. Parallel Genomic Alterations of Antigen and Payload Targets Mediate Polyclonal Acquired Clinical Resistance to Sacituzumab Govitecan in Triple-Negative Breast Cancer. Cancer Discov 2021;11(10):2436–45 doi 10.1158/2159-8290.CD-21-0702. [PubMed: 34404686]

40. Bardia A, Tolaney SM, Punie K, Loirat D, Oliveira M, Kalinsky K, et al. Biomarker analyses in the phase III ASCENT study of sacituzumab govitecan versus chemotherapy in patients with metastatic triple-negative breast cancer. Ann Oncol 2021;32(9):1148–56 doi 10.1016/j.annonc.2021.06.002. [PubMed: 34116144]

41. Zhao N, Chopra S, Trepka K, Wang YH, Sakhamuri S, Hooshdaran N, et al. CUB Domain-Containing Protein 1 (CDCP1) Is a Target for Radioligand Therapy in Castration-Resistant

Prostate Cancer, including PSMA Null Disease. Clin Cancer Res 2022;28(14):3066–75 doi 10.1158/1078-0432.CCR-21-3858. [PubMed: 35604681]

42. Forte L, Turdo F, Ghirelli C, Aiello P, Casalini P, Iorio MV, et al. The PDGFRbeta/ERK1/2 pathway regulates CDCP1 expression in triple-negative breast cancer. BMC Cancer 2018;18(1):586 doi 10.1186/s12885-018-4500-9. [PubMed: 29792166]

43. Bamias A, Bowles MJ, Krausz T, Williams G, Epenetos AA. Intravesical administration of indium-111-labelled HMFG2 monoclonal antibody in superficial bladder carcinomas. Int J Cancer 1993;54(6):899–903 doi 10.1002/ijc.2910540604. [PubMed: 8335396]

44. Zorzos J, Skarlos DV, Epenetos AA, Pectasides D, Koutsioumba P, Elemenoglou J, et al. Intravesical administration of tumor-associated monoclonal antibody AUA1 in transitional cell carcinoma of the bladder: a study of biodistribution. Urol Res 1993;21(6):435–8 doi 10.1007/BF00300082. [PubMed: 8171767]

45. Zorzos J, Skarlos DV, Pozatzidou P, Zizi A, Bakiras A, Koritsiadis S, et al. Immunoscintigraphy with iodine-131-labelled monoclonal antibody AUA1 in patients with transitional cell carcinoma of the bladder. Urol Res 1994;22(5):323–7 doi 10.1007/BF00297203. [PubMed: 7879319]

46. Pfost B, Seidl C, Autenrieth M, Saur D, Bruchertseifer F, Morgenstern A, et al. Intravesical alpha-radioimmunotherapy with 213Bi-anti-EGFR-mAb defeats human bladder carcinoma in xenografted nude mice. J Nucl Med 2009;50(10):1700–8 doi 10.2967/jnumed.109.065961. [PubMed: 19793735]
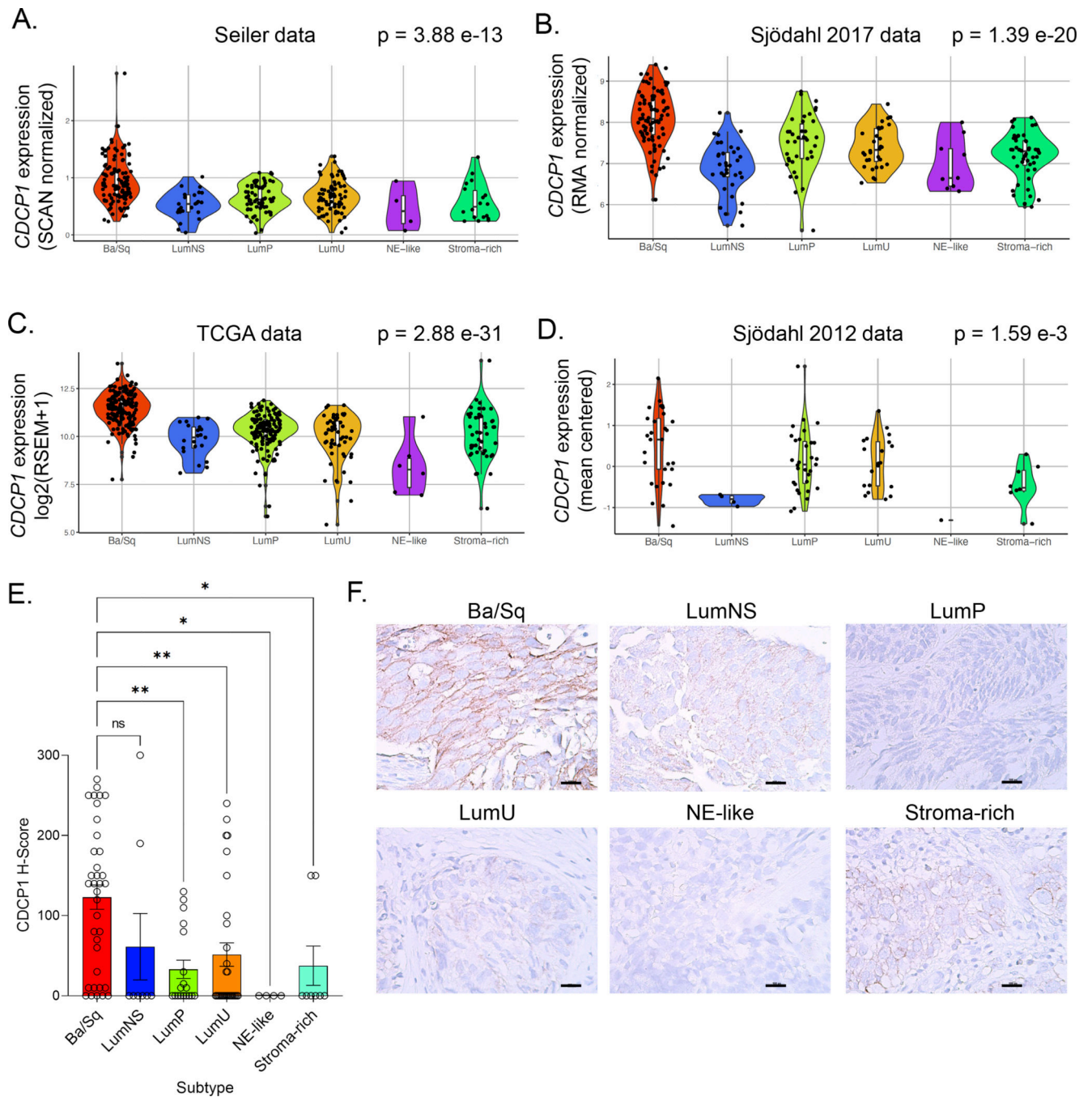
**Figure 1. CDCP1 expression across the consensus molecular subtypes of MIBC.**
A-D. Violin plots showing CDCP1 mRNA expression levels by consensus molecular subtypes in the TCGA, Seiler 2017, Sjödahl 2017, and Sjödahl 2012 cohorts. The p values from ANOVA testing for each cohort are shown, and p values from Kruskal-Wallis testing and pairwise comparisons using the Wilcoxon rank-sum test are shown in Supplemental Table 1. **E.** H-scores quantifying CDCP1 expression from primary bladder cancer biopsies. The biopsies are organized according to consensus subtype. **F.** Representative IHC images showing the membranous staining of CDCP1 in bladder cancer biopsies.
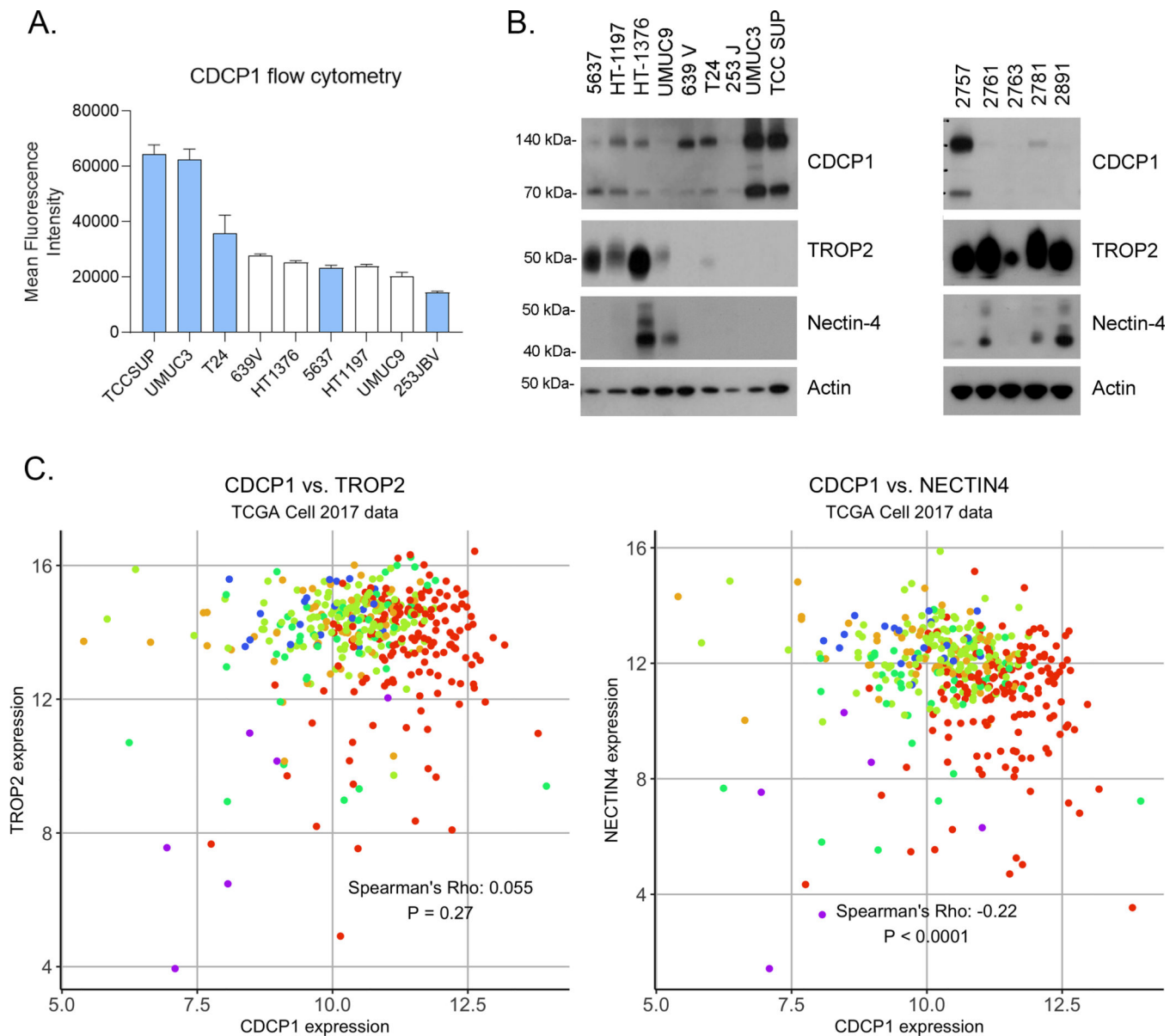
Figure 2. CDCP1 protein is expressed in human BC, including TROP2 and/or Nectin-4 null samples.
A. Flow cytometry showing the relative expression of CDCP1 on the surface of luminal (white) and basal (cyan) BC models. **B.** Immunoblot data showing the expression of intact (140 kDa) and proteolytically cleaved (70 kDa) CDCP1 in several luminal and basal human BC cell lines and PDX tissues. TROP2 and Nectin-4 immunoblot highlight the discordance with CDCP1 expression. **C.** Scatter plots show the mRNA expression of existing ADC targets Nectin-4 and TROP2 versus CDCP1 in the TCGA cohorts. The Spearman rank correlation coefficient and p-values are shown for each analysis. No correlation was observed in the Sjödahl 2012, Sjödahl 2017, and Seiler 2017 cohorts (Supplemental Figure 3). Each biopsy is color coded by molecular subtype using the system outlined in Figure 1.
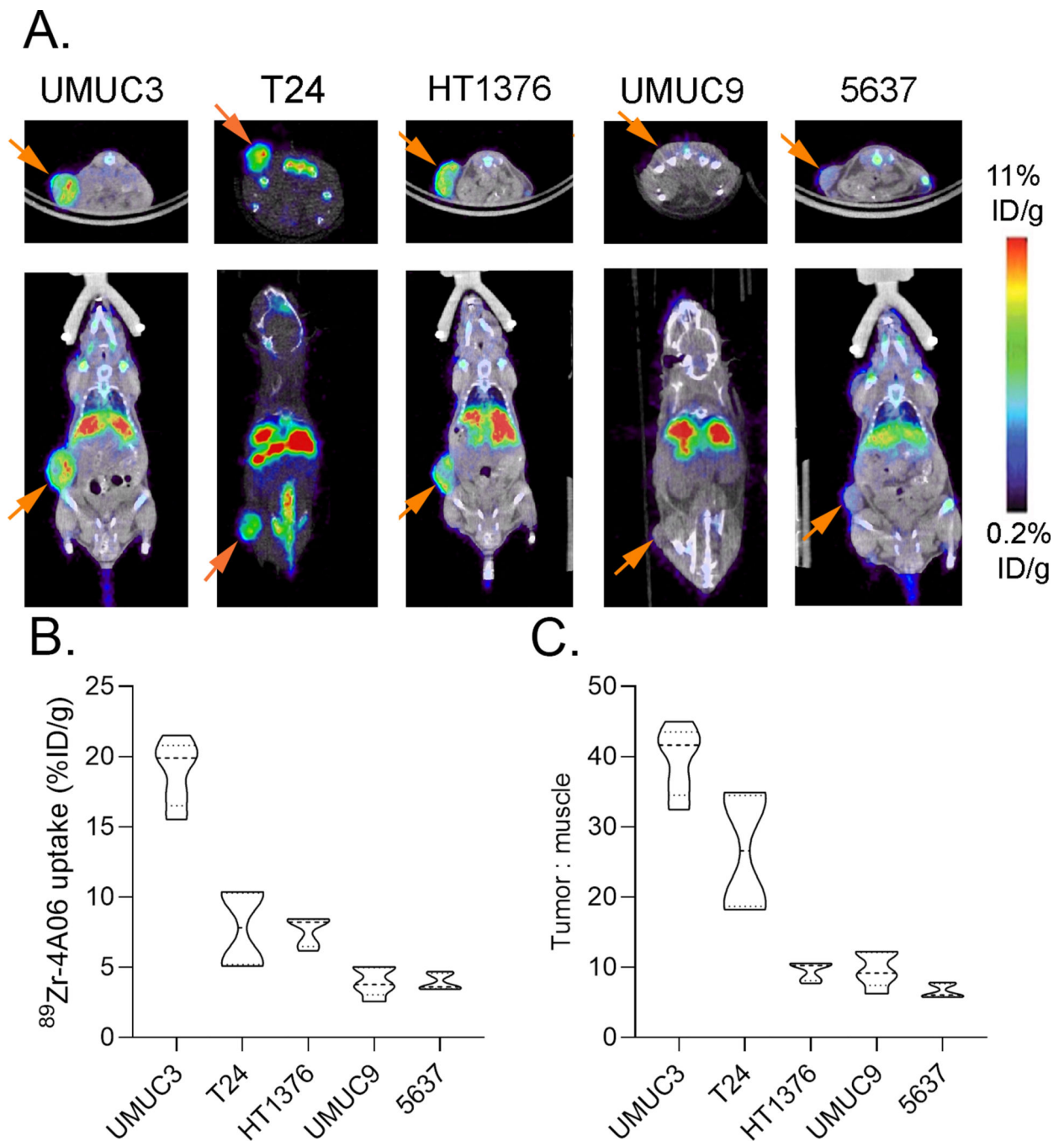
Figure 3. ^{89}Zr-4A06 PET detects molecularly diverse human BC xenografts with varying levels of CDCP1 expression.

A. Representative coronal and transverse PET/CT images acquired 72 hours post injection of ^{89}Zr-4A06. The position of the tumor is indicated with an orange arrow. **B.** Ex vivo tumor uptake data acquired 72 hours post injection of ^{89}Zr-4A06 (n = 5 mice/tumor). **C.** Tumor to muscle ratios calculated from postmortem biodistribution data collected 72 hours post injection.
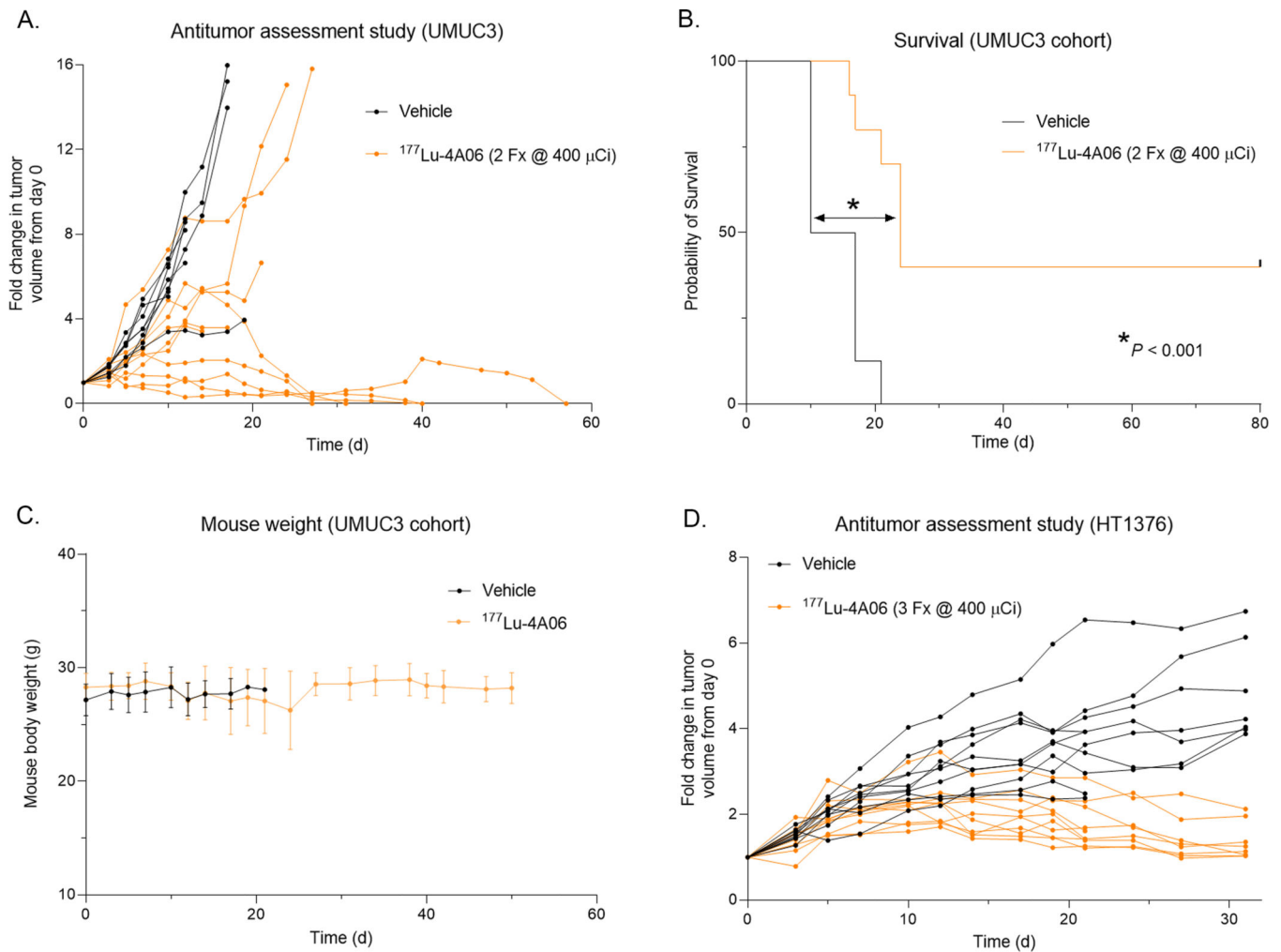
Figure 4. Treatment with ^{177}Lu-4A06 suppresses BC tumor growth.
A. Growth curves collected from mice bearing subcutaneous UMUC3 xenografts post treatment with vehicle or a fractionated dose of ^{177}Lu-4A06 (2 doses of 400 μCi/dose, day 0 and day 7, n = 9 mice/arm). The mean tumor volume was significantly smaller in the treated versus vehicle group by day 20 of the study. **B.** A Kaplan-Meier curve showing relative survival in the vehicle versus treated arms. ^{177}Lu-4A06 significantly extended survival compared to control. P < 0.01. Four of nine mice in the treated arm experienced complete tumor regressions and no regrowth was documented out to 120 days post injection. **C.** Mouse weight measurements from mice in the UMUC3 cohort that received vehicle of ^{177}Lu-4A06. **D.** Growth curves collected from mice bearing subcutaneous HT1376 xenografts post treatment with vehicle or a fractionated dose of ^{177}Lu-4A06 (2 doses of 400 μCi/dose, day 0 and day 7, n = 8 mice/arm). The mean tumor volume was significantly smaller in the treated versus vehicle group by day 10 of the study.
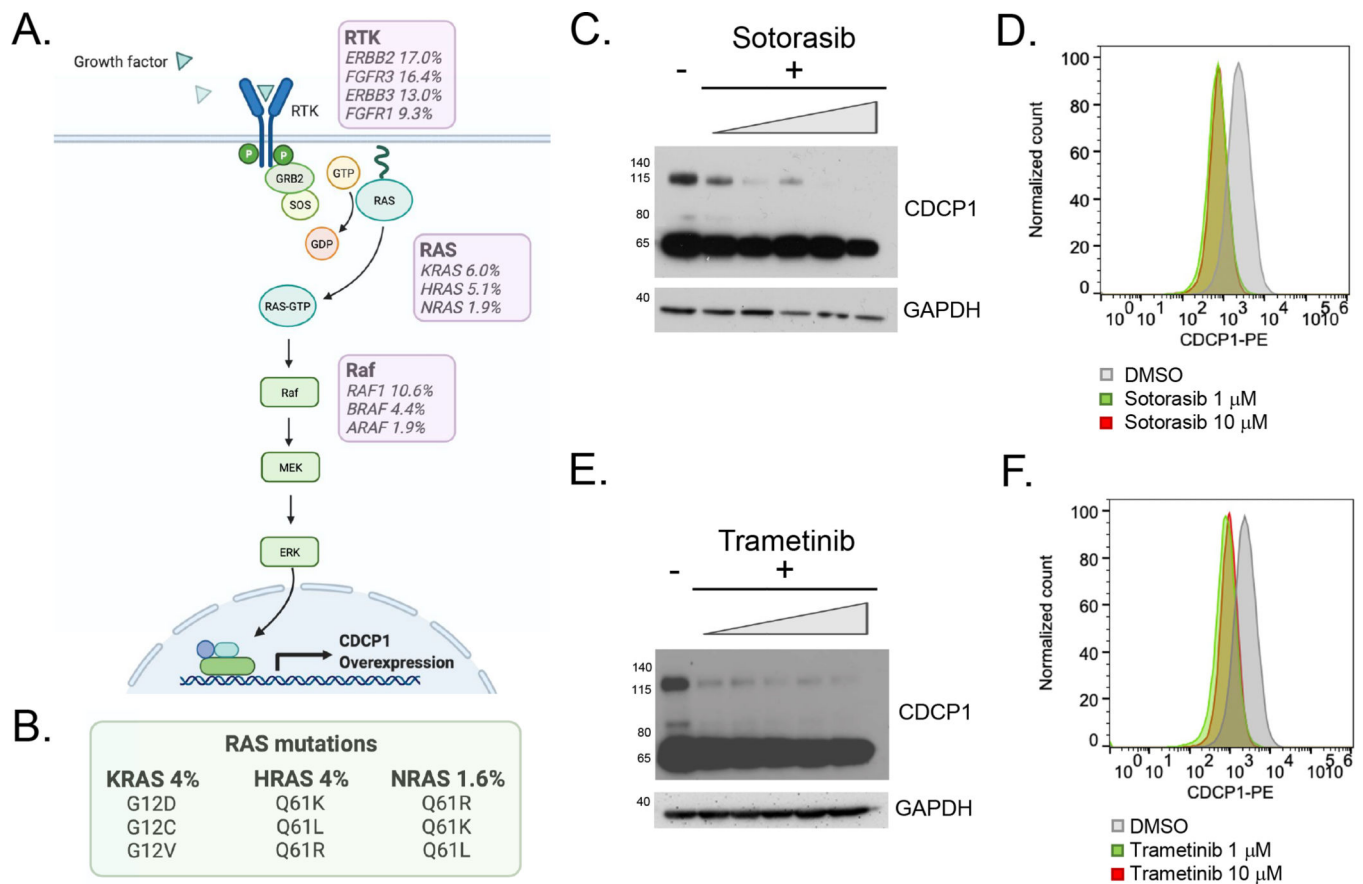
Figure 5. CDCP1 expression is regulated by the RAS-Raf-MEK signaling pathway in BC.
A. Diagram showing the RAS-Raf-MEK pathway downstream of receptor tyrosine kinase
(RTK) signaling. The prevalence of molecular alterations (including mutations, structural
variants and copy number alterations) in bladder cancer from cbioportal is indicated in the
purple boxes. **B.** The prevalence of the most common RAS mutations in bladder cancer
from cbioportal is indicated. **C.** Western blots showing total CDCP1 expression in UMUC3
cells treated with increasing concentrations of sotorasib, a KRAS G12C inhibitor. **D.** Flow
cytometry data showing that cell surface CDCP1 expression after treatment with 1 or 10 μm
sotorasib. **E.** Western blots showing total CDCP1 expression in UMUC3 cells treated with
increasing concentrations of trametinib, a MEK inhibitor. **F.** Flow cytometry showing cell
surface CDCP1 expression after treatment with 1 or 10 μm of trametinib.

Table 1.

A summary of the CDCP1 receptor density on human bladder cancer cell lines using [125]I-4A06.

Cell Line	Bmax (fmol/mg)	95% CI	Kd (nM)	95% CI	R^2	Receptors/cell
UMUC3	27,301	22,918 – 32,291	1.84	1.0 – 3.2	0.95	1.49×10^6
TCC SUP	23,784	20,987 – 26,796	0.583	0.33 – 0.96	0.9	1.29×10^6
5637	10,037	9,390 – 10,711	0.284	0.19 – 0.39	0.94	5.48×10^5
HT1376	5,189	4,518 – 5,942	0.902	0.99 – 1.57	0.93	2.88×10^5
UMUC9	3,961	3,253 – 4,860	0.181	0.056 – 0.45	0.88	2.16×10^5